Face Centered Cubic Photonic Bandgap Materials Based on Opal-Semiconductor Composites

H. Míguez, A. Blanco, C. López, F. Meseguer, H. M. Yates, M. E. Pemble, F. López-Tejeira, F. J. García-Vidal, and J. Sánchez-Dehesa

***Abstract*— We discuss photonic crystal properties of semiconductor-opal composites and explore the possibility of using these structures as photonic bandgap (PBG) materials in the visible and near-infrared region of the spectrum. Integrated reflectance in the optical region is used to show that the photonic crystal behavior of InP-opal is enhanced with respect to the bare matrix as a result of the new refractive index contrast. Order-N band structure and transfer matrix calculations have proved to be in good agreement with the experiments. In addition, a strong coupling effect has been observed between CdS photoluminescence and the photonic structure, which leads to a partial inhibition of the spontaneous emission.**

***Index Terms*— CdS, InP, luminescence, opals, photonic bandgap (PBG), photonic crystal, semiconductor.**

I. Introduction

WHEN THE idea of photonic bandgap (PBG) materials was introduced a decade ago, the door to an unexplored field in materials science was opened [1], [2]. Prediction concerning their promising properties immediately gave rise to a large and ever increasing number of theoretical and experimental studies. One of the main aims of PBG technology is the fabrication of three-dimensional (3-D) system in the visible and infrared (IR) region of the electromagnetic spectrum. Several different routes have been proposed in order to attain this goal. The most extended method is the micromachining of a bulk material by lithographic methods. Very recently, two groups [3], [4] have built up to seven monolayers of a PBG crystal with a diamond-like symmetry working in the near-infrared region of the EM spectrum. Also, great attention has been paid to the photonic crystal behavior of solid crystals of colloidal particles, which have proved to be good candidates for PBG materials [5]. Recently, solid ordered arrangements of latex [6] and silica [7], [8] particles have been used as a template to fabricate inverse opals. Although in these works there are no evidences of a full gap, they constitute elegant examples of the route to be followed in the search for opalline materials with a sizable full gap.

Here, we show how to fabricate bare opals of high-quality whose pseudogap is tunable in the VIS and NIR region of the EM spectrum. Moreover, by infilling the bare opal matrix with high dielectric constant semiconductors, such as InP ($\varepsilon = 12.25$), the photonic crystal properties of the opal structure can be improved. Finally, we show how the light emission properties of an embedded semiconductor, e.g., CdS, can be dramatically modified by the presence of the dielectric superstructure.

The fabrication of opal-based PBG materials requires the following steps:

1) synthesis of monodisperse submicrometric silica particles (we note that in order to tune pseudogaps over a large region of the EM spectrum (visible and IR) it would be necessary to control the diameter of silica spheres over an ample range of values);
2) 3-D periodic packing;
3) sintering processing to give the samples mechanical stability and also, to control the interparticle pore volume and thereby the filling fraction;
4) synthesis of high refractive index materials within the voids of the opal to increase the refractive index contrast.

II. Fabrication of Artificial Opals

The quality of the opalline structure dramatically depends on the monodispersity of the starting particles. Therefore, the first requirement in order to build technologically interesting materials is to control the production of well-shaped size-controlled spherical silica particles. The synthesis of submicron silica particles has been extensively studied [9], [10]. The most common method is that developed by Stöber *et al.* [11]. It consists of a sol-gel process in which a Si alkoxide compound is hydrolyzed creating Si–O chains which condense to form amorphous silica nanoparticles. Under controlled reaction conditions, monodisperse spheres (less than 5% in dispersion) with diameters in the range of 200–700 nm can be produced.

Manuscript received March 25, 1999; revised August 17, 1999. This work was supported in part by the Spanish CICyT Project MAT97-0698-C04, the Generalitat Valenciana, the Fundación Ramón Areces, and EU Project PHOBOS-27731.

H. Míguez, A. Blanco, and C. López are with the Instituto de Ciencia de Materiales de Madrid (Consejo Superior de Investigaciones Científicas), Cantoblanco 28049 Madrid, Spain.

F. Meseguer is with the Instituto de Ciencia de Materiales de Madrid (Consejo Superior de Investigaciones Científicas), Cantoblanco 28049 Madrid, Spain. He is also with Unidad Asociada CSIC-UPV, Departamento de Física Aplicada. E.T.S. Arquitectura, Universidad Politécnica de Valencia, Valencia 46022 Spain (e-mail: fmese@fis.upv.es).

H. M. Yates and M. E. Pemble are with the Department of Chemistry, University of Salford, Salford, Manchester M5 4WT U.K.

F. López-Tejeira, F. J. García-Vidal, and J. Sánchez-Dehesa are with the Departamento de Física Teórica de la Materia Condensada, Facultad de Ciencias, Universidad Autónoma de Madrid, Madrid 28049 Spain.

Publisher Item Identifier S 0733-8724(99)08810-6.

After synthesis, a colloidal suspension (with a typical concentration of 10^{10} particles/cm^3) is left to settle under gravity. Sedimentation velocity follows Stokes law [12], which indicates that the particles do not stick together, but rather sediment as single particles. This is due to the fact that these particles behave as hard spheres, with no interaction, which could give rise to flocculation. There are two main conditions which must be fulfilled to ensure that sedimentation gives rise to a good quality crystalline structure. First, the suspension concentration should be low enough to allow single particle behavior [13]–[15]. Second, Brownian and gravitational energy should be of the same order. Under these conditions, particles arriving at the growing sedimentary surface may sample many possible sites before stopping at the position of minimum potential energy [16]. Opal crystal growth processes have been shown to follow the Edwards–Wilkinson model [17], which means that they take place extremely close to the equilibrium. When all the particles have settled, the sediment is carefully dried and later removed from the substrate. It constitutes a so-called "green" or as-grown opal sample.

An analysis of the crystalline structure of artificial opals has recently shown that they present face centered cubic (fcc) packing rather than a hexagonal close packed (hcp) structure or any mixture thereof [18]. This result is in agreement with computer simulations recently performed by Woodcock [19]. In Fig. 1, two scanning electron microscopy (SEM) images of a sample made of 480-nm spheres are shown. The images correspond to internal facets of the sample obtained after cleavage. A large terrace between the {111} and {100} crystalline planes can be seen in Fig. 1(a), while a detail of the structure of a {110} facet is shown in Fig. 1(b).

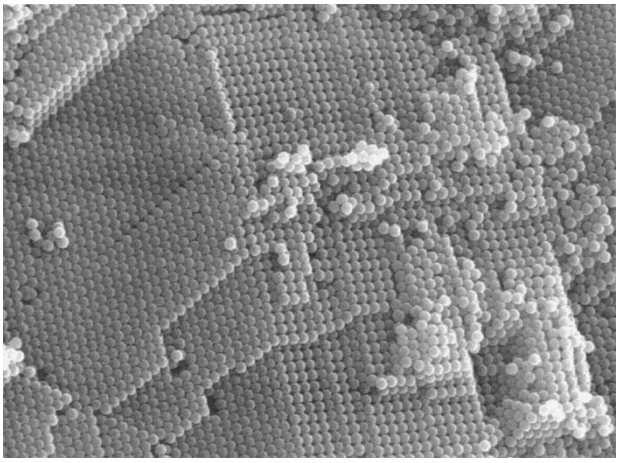

(a)

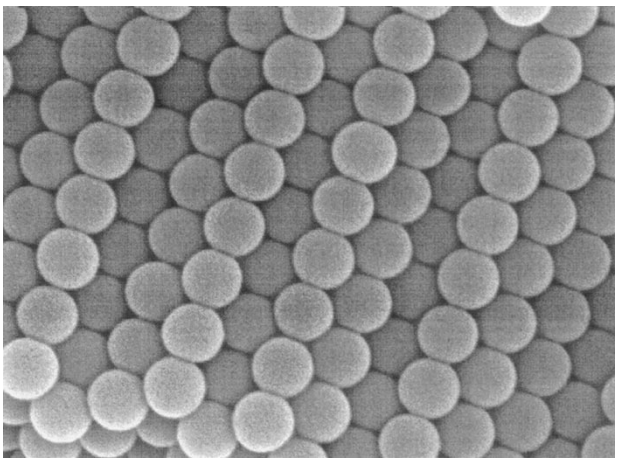

(b)

Fig. 1. SEM images of a cleft edge of an artificial opal made of 480-nm spheres: (a) a large terrace between {111} and {100} set of planes is observed and (b) detail of {110} planes are shown.

III. Sintering and Filling Factor Control

As-grown opals are solid but present a low mechanical stability, which can be greatly improved by a sintering process [12]. Furthermore, this process allows the opal filling fraction (ff) to be controlled and therefore its optical properties and the accessible pore volume [20]. The latter of which is an important parameter in order to use artificial opals as hosts for other materials. Green samples present a ff of about 60%, which implies that they are very open structures. Hardly, any structural difference can be observed (by SEM) between as-grown opals and those annealed at temperatures up to 950 °C for 3 h. Nevertheless, dramatic changes in the optical features and the mechanical stability take place. These changes are caused by modifications in the physico-chemical characteristics of the sphere surfaces. A mild sintering, promoted by the incipient viscous flow, causes the formation of necks between the spheres when the temperature is between 700 and 950 °C. In this region, opals present a filling fraction of 74%. Above 950 °C, however, strong structural and optical modifications take place. Above this firing temperature the pore volume reduces as spheres start crushing into each other. The morphological outcome of such particle interpenetration can be observed in the SEM image given in Fig. 2. An internal {111} type facet, obtained after cleavage, of an artificial opal sintered at 1015 °C for 6 h presents fractures or holes that indicate the location of the particles belonging to the plane lying above. These images show that the strong structural modification that takes place does not influence the long-range order existing in the material.

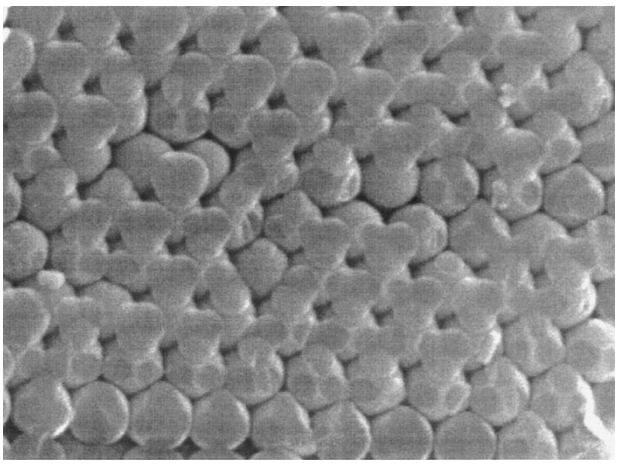

Fig. 2. SEM image of an internal {111} facet of an artificial opal made of 415-nm spheres and sintered up to 1015 °C for 6 h. Remains left behind and some bits missing from the spheres in the plane are the signatures of the spheres lying above and separated on cleavage.

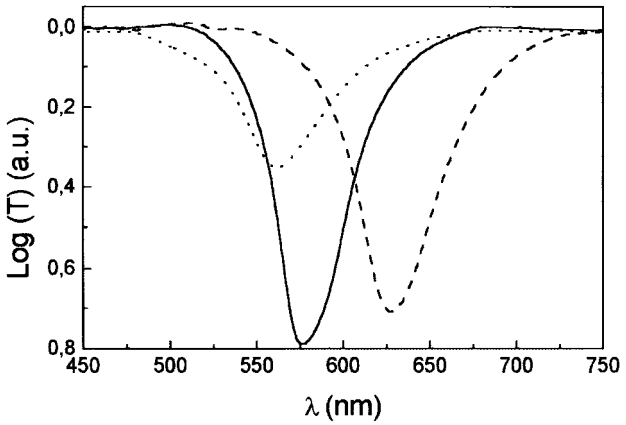

Fig. 3. Optical transmission at normal incidence with respect to the {111} planes of an opal made of 260-nm spheres as-grown (dashed line), sintered at 950 °C (solid line) and sintered at 1050 °C (dotted line).

Both contraction (below 700 °C) and interpenetration (above 900 °C) cause a reduction of the pore size, thus increasing the filling factor of the structure. By sintering, it is possible to properly control the filling factor of the structure between 74%, corresponding to a compact structure, and 100%, which corresponds to a system without pores (samples treated at $T = 1100$ °C). As a consequence, the Bragg diffraction coming from the sample undergoes a blue shift as the annealing temperature increases. This can be seen in Fig. 3, in which the optical transmission spectra at normal incidence with respect to the (111) set of planes of the same opal annealed at different temperatures are shown. All these results demonstrate that certain photonic crystal properties of artificial silica opals can be easily and accurately controlled by means of a thermal treatment.

IV. Photonic Crystal Behavior of Bare Opals

Concerning the photonic crystal behavior of bare opals, it has been shown that the lattice parameter of these structures, and therefore, their optical properties can be easily tuned through the sphere size. This can be done for sphere diameters between 200 amd 700 nm; thus covering the whole visible and near infrared regions [21]. Optical transmission spectra for seven different sintered (950 °, ff = 74%) opals are shown in Fig. 4. In all cases, the large dip in transmission corresponds to the (111) Bragg reflection. The position (in nanometers) of the (111) Bragg diffraction peak shifts linearly toward lower wavelengths as the sphere diameter decreases, consistent with Bragg law for normal incidence.

Through the sphere size, the pseudogap of the artificial opals can be tuned to match the electronic bandgap (where optical emission takes place) of most semiconductors or the emission bands of many dyes. In this way, their luminescence properties can be altered and controlled. In the next section, we will discuss how, in semiconductor-opal composites, one can thus couple electronic and optical properties. Besides, provided a large enough dielectric contrast was achieved by infilling the opal voids and a full PBG material was obtained, one could tune the full gap to any desired region of the spectrum.

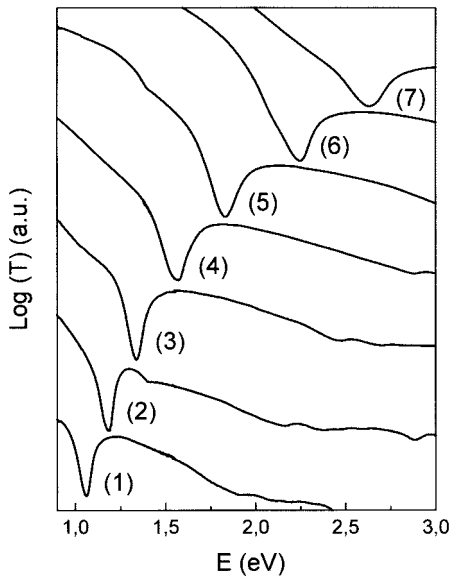

Fig. 4. Optical transmission at $\theta = 0°$ for opal-like structures made of spheres with different diameter: (1) 535 nm, (2) 480 nm, (3) 415 nm, (4) 350 nm, (5) 305 nm, (6) 245 nm, and (7) 220 nm. The spectra have been vertically shifted for the sake of clarity.

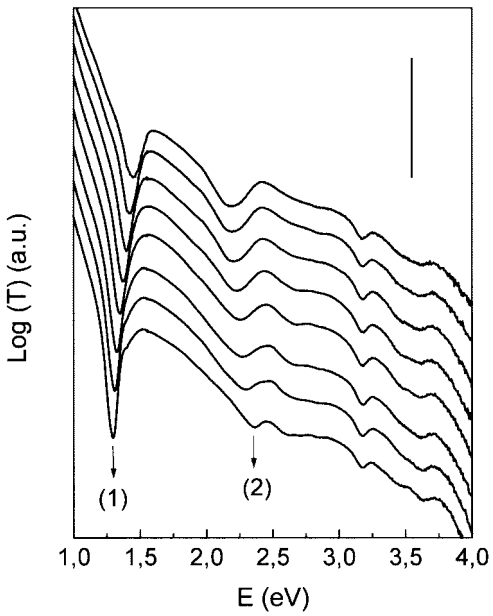

Fig. 5. Transmission spectra for different incidence angles, θ, with respect to the surface normal in a sample made of 440-nm diameter spheres. From bottom to top, $\theta = 0$, 10, 15, 20, 25, 30, 35, and 40°. The vertical bar indicates one decade. The spectra have been vertically shifted for the sake of clarity.

It has also been shown that bare opals present a photonic pseudogap [21]. Optical transmission measurements performed at different incidence angles of white light with respect to the {111} set of planes, such as those shown in Fig. 5, indicate that a different range of frequencies is not allowed to propagate through the opal. Both first and second pseudogaps can be observed. The low dielectric constant contrast and the high filling fraction of the opal structure are responsible for the absence of a full gap, even when the symmetry is appropriate [22], [23].

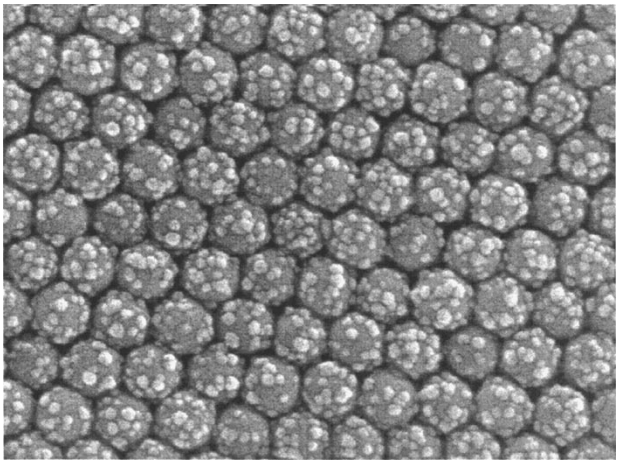

Fig. 6. Scanning electron micrograph of a {111} surface of an artificial opal infilled with InP. InP crystallites can be seen on the surface of the spheres.

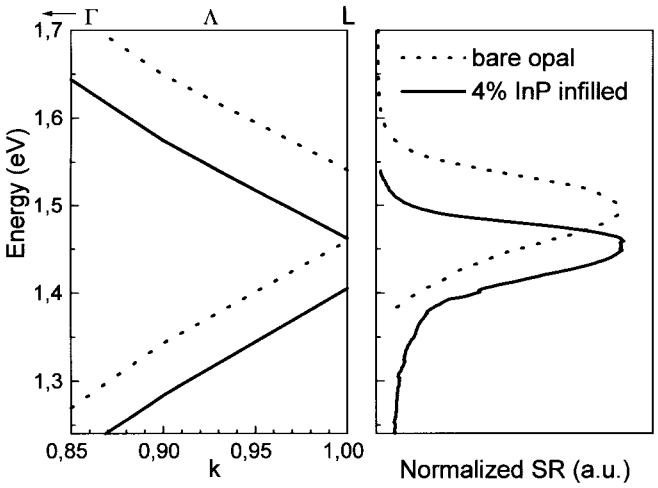

Fig. 7. (a) Theoretically calculated photonic bands at the vicinity of the L point and (b) normalized specular reflectance of a bare opal made of 380-nm diameter spheres (dotted lines) and the same opal after infilling with InP a 4% of the pore volume (solid lines).

V. Photonic Bandgap Behavior of Semiconductor Infilled Artificial Opals

Semiconductor infilling can, therefore, be used in order to either increase PBG properties or to inhibit spontaneous emission of the guest or both. The loading of semiconductors within the opal has many advantages compared to other materials. First, because of the large dielectric constant of bulk semiconductors, which would enhance the dielectric contrast of the composite. Second, due to the highly efficient band-to-band emission of the semiconductor, which would allow the effect of the photonic bands on the spontaneous emission coming from inside the periodic dielectrics to be tested. For all the reasons above, we have infilled III–V [24] and II–VI [25] semiconductors within the pore lattice of opals.

A high dielectric constant semiconductor, InP ($\varepsilon = 12.25$), has been infilled in order to enhance the efficiency of the photonic bands observed in the bare opal. The method employed to infill was metal organic chemical vapor deposition, and the whole procedure can be found elsewhere [26]. In Fig. 6, an image of {111} facet of an InP infilled opal is shown. The loading, in this case, fills 4% of the total void volume. SEM images demonstrate that the InP is very homogeneously distributed inside the matrix and, as a consequence, the guest material inherits the 3-D periodicity of the host.

We have calculated the photonic band structure along the Gamma-L direction by using an order-N method [27]. The fcc structure is represented by a cubic unit cell with a basis of five silica spheres ($\varepsilon = 2.1$). A uniform grid of $26 \times 26 \times 26$ points is employed to obtain good convergence in the results. The InP loading has been simulated assuming that the semiconductor uniformly covers the silica spheres up to the pore volume infilled.

In Fig. 7 both the calculated band structure near the L-point [Fig. 7(a)] and the normalized spectra measured [Fig. 7(b)] for a 380-nm spheres bare opal and the same opal with InP (4% of the total void volume) are shown. It is clearly seen that experimental features regarding either the peak positions as well.

In Fig. 8 (low panel), reflectance spectra of both bare opals with different particle size, and infilled with InP (filling level 4% in all cases) are shown. White light impinges with a 3° angle with respect to (111) planes in this case. In spite of the small concentration of semiconductors, the intensity of the (111) diffraction peak from the composite is twice as large as that coming from the bare structure. This result is caused by the increase in the dielectric contrast of the structure. In addition, the (111) band shifts toward larger wavelengths as a result of the average dielectric constant increase. Another interesting feature concerns the tunability of the PBG. The Bragg peak arising from the opal-semiconductor composite can be tuned across the InP fundamental absorption edge simply by varying the diameter of the silica spheres.

We have also performed a calculation of the reflectance spectra using a transfer matrix formalism [28]. Now, a prismatic cell is employed to reproduce the opal orientation along the (111)-direction. Good accuracy is obtained using a grid of $7 \times 13 \times 18$ points. The theoretical spectra shown in the upper panel of Fig. 8 have been calculated considering the frequency dependence of the InP dielectric function $\varepsilon(\omega)$, which has been fitted from their corresponding bulk values [29], and we have assumed a sample thickness of 128 unit cells. It is remarkable the good agreement between theory and experiment regarding the peak positions, their widths, and even their relative change in height when the semiconductor is loaded. Diffuse reflectance produced by the different types of disorder and/or defects existing in our samples could be the origin of the background reflectance observed in the experiments that is not reproduced by our calculations. The comparison between the experimental spectra for both the bare opal sample and the one InP loaded indicate that the semiconductor infilling produces the quenching of the background reflectance and enhances the photonic properties of the opal.

Finally, we turn our attention to the effects that opal-based photonic crystals have on the luminescence of guest materials. Inhibition of the spontaneous emission is a must when it comes to building lasers with a low threshold. Recently,

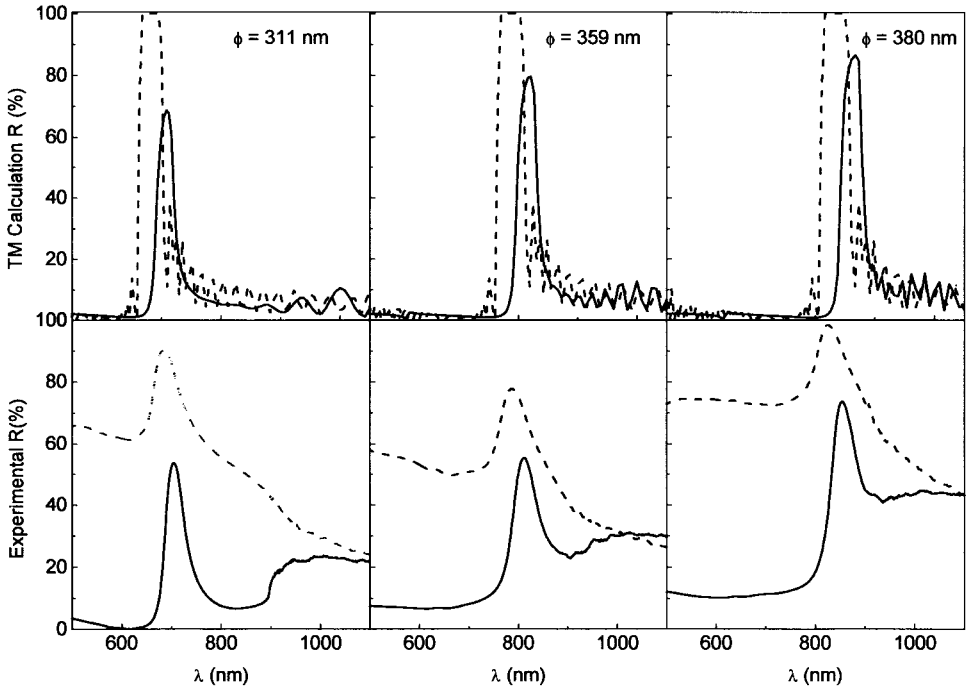

Fig. 8. Lower panel: integrated reflectance of bare (solid line) and InP loaded (dashed line) opals (4 vol.% of the pore volume). Three cases are shown for opals of increasing diameter: 311, 359, and 380 nm. Upper panel: theoretical calculation for the bare and infilled opals shown in the lower panel.

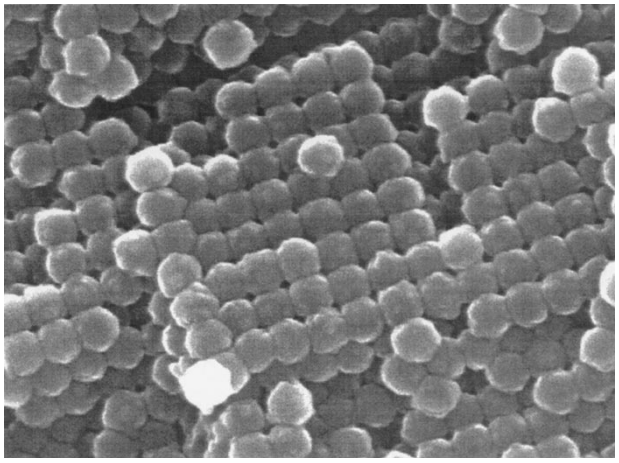

Fig. 9. SEM image of internal {100} facets obtained from a cleft edge of a CdS embedded opal.

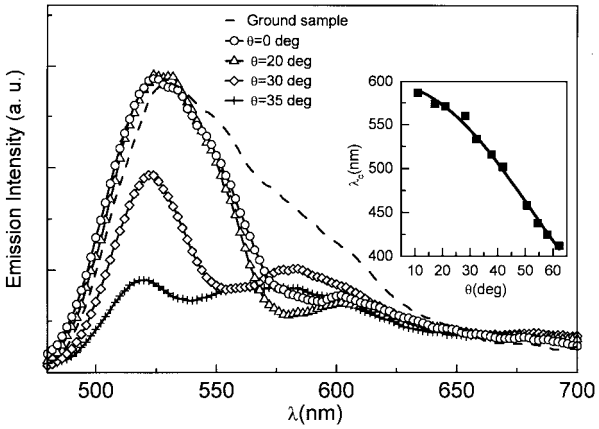

Fig. 10. Photoluminescence spectra at different collection angles for a CdS infilled opal and the same opal grounded (dashed line). As the sample is tilted the dip in the emission shifts following the Bragg law (inset).

a number of studies concerning the effect of silica opals on the luminescence of lucent materials (organic dyes and semiconductors) have been performed [25], [30], [31]. In order to examine further this effect, we have synthesized CdS in the opal voids employing a chemical bath deposition method. Fig. 9 shows an image of a 100 facet of a sample infilled with CdS to 23% of the pore volume. It can be seen that CdS crystals are uniformly distributed inside the sample. Transmission spectra at normal incidence of bare and CdS infilled opals (not shown here) allow us to estimate the amount of infilled CdS. Concerning luminescence, none has been observed from bare opals. However, when a bare opal is CdS loaded, a clear emission band centered at 530 nm can be detected. A judicious choice of sphere size and CdS content allows us to match the photonic pseudogap of the opal to the CdS emission, so that photonic crystal effects of the host can be observed. For a sample of 260-nm spheres, the forbidden band for normal incidence appears at 580 nm, well within the emission band. The effect of the host on the luminescence of the guest CdS can be seen in Fig. 10. The luminescence of a ground-up CdS infiltrated opal is shown as well for comparison. A series of luminescence spectra obtained as the sample is rotated are shown, and a clear dip is detected in each emission spectrum. When the sample is tilted the dip in the emission shifts toward lower wavelengths, according to the Bragg law (inset in Fig. 10), sweeping across the emission band. These dips coincide with the transmission minima (stop bands) of the ordered structure. When the sample is ground and the order vanishes from the system, the luminescence recovers the original CdS line-shape and photonic effects are lost. This

demonstrates the partial inhibition of the emission produced by the photonic structure of the host.

VI. Conclusions

Structures based on opals prove to be a valid method for the development of PBG materials in the visible and NIR regions of the EM spectrum. We have fabricated high-quality bare opals with sphere sizes covering the range between 200 and 700 nm. This allows us to tune the (111) pseudogap through the visible and NIR regions of EM spectrum. Sintering gives rises to mechanical stability and permits the pore size of bare opals, as well as their optical properties, to be controlled. In addition to this, semiconductor infilling methods have been developed. A strong enhancement of the photonic bands has been achieved by InP infilling within the opal void lattice. In addition, a clear modification of the luminescence of CdS embedded opals due to the host structure has been observed. Although these results are not conclusive, they represent a substantial first step along the pathway leading to the fabrication of full gap PBG materials based on artificial opals.

Acknowledgment

The authors would like to thank A. Cintas for her help in silica colloid synthesis and M. Planes for his help during SEM characterization.

References

[1] E. Yablonovitch, "Inhibited spontaneous emission in solid state physics and electronics," *Phys. Rev. Lett.*, vol. 58, p. 2059, 1987.
[2] S. John, "Strong localization of photons in certain disordered dielectric superlattices," *Phys. Rev. Lett.*, vol. 58, p. 2486, 1987.
[3] N. Yamamoto, S. Noda, and A. Chutinan, "Development of one period of a three dimensional photonic crystal in the 5-10 m wavelength region by wafer fusion and laser beam diffraction pattern observation technique," *Jpn. J. Appl. Phys.*, vol. 37, p. L1052, 1998.
[4] S. J. Lin, J. G. Fleming, D. L. Hetherington, B. K. Smith, R. Biswas, K. M. Ho, M. M. Sigalas, W. Zubrzycki, S. R. Kurtz, and J. Bur, "A three-dimensional photonic crystal operating at infrared wavelengths," *Nature*, vol. 394, p. 251, 1998.
[5] F. Meseguer, H. Míguez, A. Blanco, and C. López, "Photonic band gap materials based on opal-like structures," in *Applied Physics Series, Transworld Research Network*, M. Pandalai, Ed., in press.
[6] J. E. G. J. Wijnhoven and W. L. Vos, "Preparation of photonic crystals made of air spheres in titania," *Science*, vol. 281, p. 802, 1998.
[7] A. A. Zakhidov, R. H. Baughman, Iqbal, Z. C. Cui, I. Khayrullin, S. O. Dantas, J. Martí, and V. G. Ralchenko, "Carbon strutures with three-dimensional periodicity at optical wavelengths," *Science*, vol. 282, p. 897, 1998.
[8] Y. A. Vlasov, N. Yao, and D. J. Norris, "Synthesis of photonic crystals for optical wavelengths from semiconductior quantum dots," *Adv. Mater.*, vol. 11, p. 165, 1999.
[9] C. J. Brinker and G. W. Scherer, *Sol-Gel Science.* New York: Academic, 1990.
[10] *The Colloid Chemistry of Silica*, H. E. Bergna, Ed. Washingon, DC: Amer. Chem. Soc., 1994, Adv. Chem. Series, vol. 234.
[11] W. Stöber, A. Fink, and E. Bohn, "Controlled growth of monodisperse silica spheres in the micron size range," *J. Colloid Interface Sci.*, vol. 26, p. 62, 1968.
[12] R. Mayoral, J. Requena, J. S. Moya, C. López, A. Cintas, H. Míguez, F. Meseguer, L. Vázquez, M. Holgado, and A. Blanco, "3D long range ordering in a SiO_2 ubmicrometric-sphere sintered superstructure," *Adv. Mater.*, vol. 9, p. 257, 1997.
[13] P. N. Pusey, W. van Megen, P. Bartlett, B. J. Ackerson, J. G. Rarity, and S. M. Underwood, "Structure of crystals of hard colloidal spheres," *Phys. Rev. Lett.*, vol. 63, p. 2753, 1989.
[14] A. van Blaaderen and P. Wiltzius, "Real-space structure of colloidal hard-sphere glasses," *Science*, vol. 270, p. 1177, 1995.
[15] M. D. Sacks and T. Y. Tseng, "Preparation of SiO_2 glass from model powder compacts," *J. Amer. Ceram. Soc.*, vol. 67, p. 526, 1984.
[16] A. L. Barabási and H. E. Stanley, *Fractal Concepts in Surface Growth.* Cambridge, U.K.: Cambridge Univ. Press, 1995.
[17] R. C. Salvarezza, L. Vázquez, H. Míguez, R. Mayoral, C. López, and F. Meseguer, "Edward- Wilkinson behavior of crystal surfaces grown by sedimentation of SiO_2 nanospheres," *Phys. Rev. Lett.*, vol. 77, p. 4572, 1996.
[18] H. Míguez, F. Meseguer, C. López, A. Mifsud, J. S. Moya, and L. Vázquez, "Evidence of FCC crystallization of SiO_2 nanospheres," *Langmuir*, vol. 13, p. 6009, 1997.
[19] L. V. Woodcock, "Entropy difference between the face-centred cubic and hexagonal close-packed crystal structures," *Nature*, vol. 385, p. 141, 1997.
[20] H. Míguez. F. Meseguer, C. López, A. Blanco, J. S. Moya, J. Requena, A. Mifsud, and V. Fornés, "Control of photonic crystal properties of fcc packed submicrometer SiO_2 spheres by sintering," *Adv. Mater.*, vol. 10, p. 480, 1998.
[21] H. Míguez, C. López, F. Meseguer, A. Blanco, L. Vázquez, R. Mayoral, M. Ocaña, A. Mifsud, and V. Fornés, "Photonic crystal properties of packed submicrometric SiO_2 spheres," *Appl. Phys. Lett.*, vol. 71, p. 1148, 1997.
[22] For a deep theoretical description of the EM waves behavior within opals, a full photonic band structure calculation can be found in K. Busch and S. John, *Phys. Rev. E*, vol. 58, p. 3896, 1998.
[23] H. S. Sözüer, J. W. Haus, and R. Inguva, "Photonic bands: Convergence problems with the plane wave method," *Phys. Rev. B*, vol. 45, p. 13962, 1993.
[24] H. Míguez, A. Blanco, F. Meseguer, C. López, H. M. Yates, M. E. Pemble, V. Fornés, and A. Mifsud, "Bragg diffraction from indium phosphide infilled fcc silica colloidal crystals," *Phys. Rev. B*, vol. 59, p. 1563, 1999.
[25] A. Blanco, C. López, R. Mayoral, H. Míguez, F. Meseguer, A. Mifsud, and J. Herrero, "CdS luminescence inhibition by a photonic structure," *Appl. Phys. Lett.*, vol. 73, p. 1781, 1998.
[26] H. M. Yates, M. E. Pemble, H. Míguez. A. Blanco, C. López, F. Meseguer, and L. Vázquez, "Atmospheric pressure MOCVD growth of crystalline InP in opals," *J. Cryst. Growth*, vol. 193, p. 9, 1998.
[27] A. J. Ward and J. B. Pendry, "Calculating photonic Green's functions using non-orthogonal finite difference time-domain method," *Phys. Rev. B*, vol. 58, p. 7252, 1998.
[28] J. B. Pendry and A. MacKinnon, "Calculation of photon dispersion relations," *Phys. Rev. Lett.*, vol. 69, p. 2772, 1992.
[29] *Handbook of Optical Constants of Solids*, E. Palik, Ed. New York: Academic, 1998.
[30] Y. A. Vlasov, K. Luterova, I. Pelant, B. Hönerlage, and V. N. Astratov, "Enhancement of optical gain of semiconductors embedded in 3-dimensional photonic crystals," *Appl. Phys. Lett.*, vol. 71, p. 1616, 1997.
[31] E. P. Petrov, V. N. Bogomolov, I. L. Kolosha, and S. V. Gaponenko, "Spontaneous emission of organic molecules embedded in a photonic crystal," *Phys. Rev. Lett.*, vol. 81, p. 77, 1998.

H. Míguez, photograph and biography not available at the time of publication.

A. Blanco, photograph and biography not available at the time of publication.

C. López, photograph and biography not available at the time of publication.

F. Meseguer, photograph and biography not available at the time of publication.

H. M. Yates, photograph and biography not available at the time of publication.

M. E. Pemble, photograph and biography not available at the time of publication.

F. López-Tejeira, photograph and biography not available at the time of publication.

F. J. García-Vidal, photograph and biography not available at the time of publication.

J. Sánchez-Dehesa, photograph and biography not available at the time of publication.